INSTITUTE OF PHYSICS PUBLISHING JOURNAL OF PHYSICS D: APPLIED PHYSICS

J. Phys. D: Appl. Phys. **38** (2005) A39–A43 doi:10.1088/0022-3727/38/10A/008

Bragg-case limited projection topography study of surface damage in diamond-crystal plates

Y Zhong, S Krasnicki, A T Macrander[1], Y S Chu and J Maj

Advanced Photon Source, Argonne National Laboratory, Argonne, USA

E-mail: macrander@aps.anl.gov

Received 1 March 2005
Published 6 May 2005
Online at stacks.iop.org/JPhysD/38/A39

Abstract

To characterize diamond monochromators for synchrotron radiation beamlines, images for a region 25 μm below the surface were obtained. Topographical images of a Bragg-diffracted beam having a scattering angle (twice the Bragg angle) of 90° were obtained from asymmetric reflections with a CCD area detector. A 25 μm incident slit was used to section the sample topographically. Patchwork images for the full surface area, but limited in depth to the slit size, were assembled from microbeam images. The small extinction depths provided by the asymmetric reflection geometry, namely, 2.8 μm and 3.5 μm for ideal diamond crystals set for the (224) and (044) reflections, respectively, permitted data analyses for a region near the surface. The diamonds were synthetic type Ib (yellowish due to nitrogen impurities). They were in the shape of plates sized 6 × 5 mm and were 0.5 mm thick. Measurements were made using monochromatic bending magnet radiation at the Advanced Photon Source at 12.04 keV and 13.90 keV. Data obtained before and after chemical etching demonstrate that damage visible as contrast from saw grooves is largely removed by etching. Dislocation etch pits were observed after etching for the (111) surface but not for the (100) surface.

(Some figures in this article are in colour only in the electronic version)

1. Introduction

Diamonds have proved to be useful for synchrotron beamlines as beam splitters [1] and as monochromators [2]. We have previously been able to narrow the rocking-curve width of diamonds by chemical etching [3]. Stimulated by this result, we have been pursuing topographical techniques to study possible damage confined to the near-surface region, for example, damage that may result from sawing.

We employed Bragg-case diffraction. That is, we made measurements in reflection. The diffraction geometry is similar to the Bragg-case topography on diamond reported by Wierzchowski and Moore [4] and on SiGe by Wieteska and co-workers [5]. As in [5], we also used a slit to section the sample topographically. We then assembled the sectioned images into patchwork images of the entire sample. We used an asymmetric reflection and applied a window function to the CCD data in order to reject x-rays that were not diffracted from near the surface. We note that in [4] intensity even from the rear of the sample was imaged; such diffraction is cut out in our technique. We refer to the patchworking technique as a 'limited projection' method in keeping with the terminology of Lang [6], who applied slits to obtain Laue-case 'limited projection' images that corresponded to different depths in diamonds.

2. Samples

The diamonds were procured from a commercial vendor [7] and were grown by the HPHT technique [8]. We studied (100) oriented and (111) oriented diamonds. We made measurements before and after chemical etching. The chemical etching used is detailed in [3].

[1] Author to whom any correspondence should be addressed.

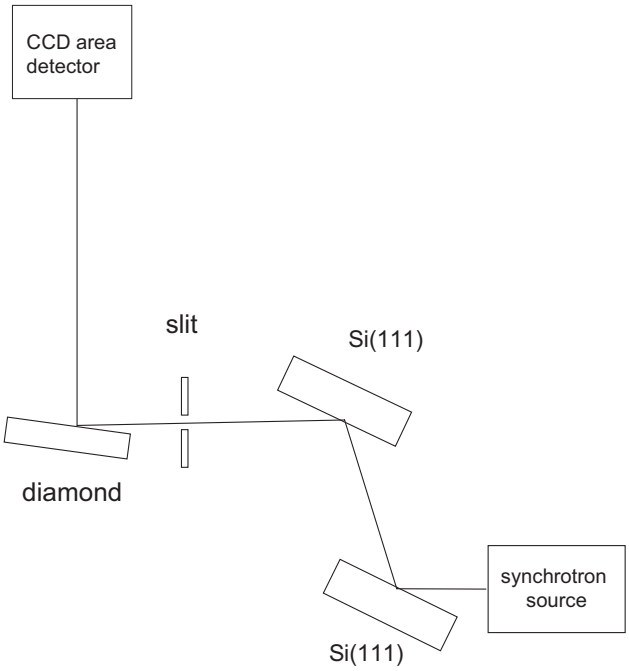

Figure 1. X-ray optical arrangement at beamline 2-BM at the Advanced Photon Source. The source of the radiation was a bending magnet followed by a harmonic rejection mirror. To obtain diffraction profiles, a double-crystal monochromator was tuned through an asymmetric reflection of a diamond. The angle for each diamond was set to a constant value for the measurements. The energy was scanned instead of the incident angle to avoid changes in the illuminated sample volume upon rotation.

3. Diffraction geometry

The studies were performed at beamline 2-BM at the Advanced Photon Source. The basic optical arrangement is shown in figure 1. The bending magnet radiation was first reflected from a mirror to remove higher harmonics and then passed through a Si(111) double crystal monochromator.

For a diamond with a (100) surface, we used the (224) reflection at 12.04 keV (0.1030 nm wavelength) to diffract at a 90° scattering angle (twice the Bragg angle) into a large-area CCD. We will refer to this case as the (100)/(224) case.

For a diamond with a (111) surface, we used the (044) reflection at 13.9 keV (0.0892 nm wavelength), which also diffracts with a 90° scattering angle. We will refer to this as the (111)/(044) case.

Both reflections were asymmetric with low incidence angles of 9° and 8° for the (100)/(224) and (111)/(044) cases, respectively. As a result of the low incidence angles, the CCD images were only slightly foreshortened from the true dimensions. Data collected in each pixel of a CCD in Bragg geometry yield spatially resolved information, as previously reported [9]. The CCD we used had 2000 × 3000 pixels having a 9 μm size with a point-spread function of 82 μm. The fibre-optic taper of the CCD was 1 : 1.

Data were obtained by tuning the monochromator through the full Bragg reflection profile of the diamonds. We chose to scan the energy to avoid changing the illuminated sample volume with rotation. The penetration depth profiles as the energy is scanned through the two reflections are shown in figure 2. Here, the penetration depth due to both extinction and absorption is plotted. The penetration at the centre of the rocking curve is only 2.8 μm for the (100)/(224) case and 3.5 μm for the (111)/(044) case.

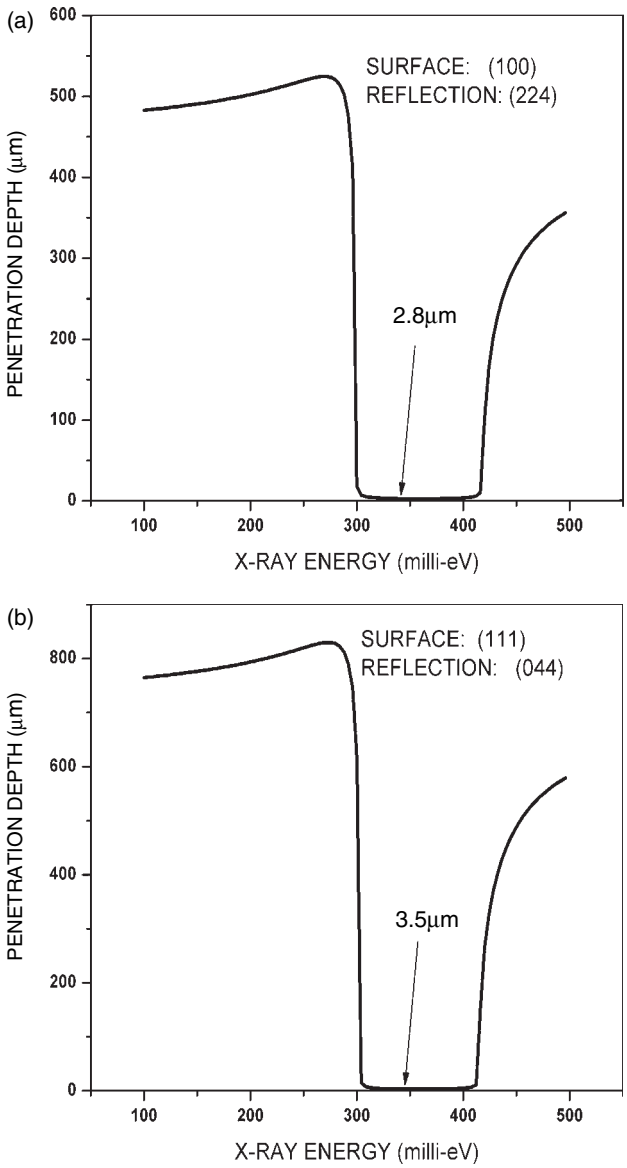

Figure 2. Diamond penetration depths according to dynamical diffraction theory. The calculations were made for an ideal diamond crystal. The Darwin width on the energy scale for ideal diamond in both cases was 0.12 eV. (*a*) A maximum penetration depth of 2.8 μm is calculated for diamonds with a (100) surface set for the asymmetric (224) reflection at 12.04 keV. The incident angle was 9°. (*b*) A maximum penetration depth of 3.5 μm is calculated for diamonds with a (111) surface set for the asymmetric (044) reflection at 13.90 keV. The incident angle was 8°.

4. Wide-beam and microbeam topographical modes

Topography images were obtained in two modes: (i) wide-beam mode, and (ii) microbeam mode. In the wide-beam mode, a very wide vertical slit opening (~800 μm) was used in front of the sample, and the topographical exposures covered the entire sample in a single exposure. For all our wide-beam

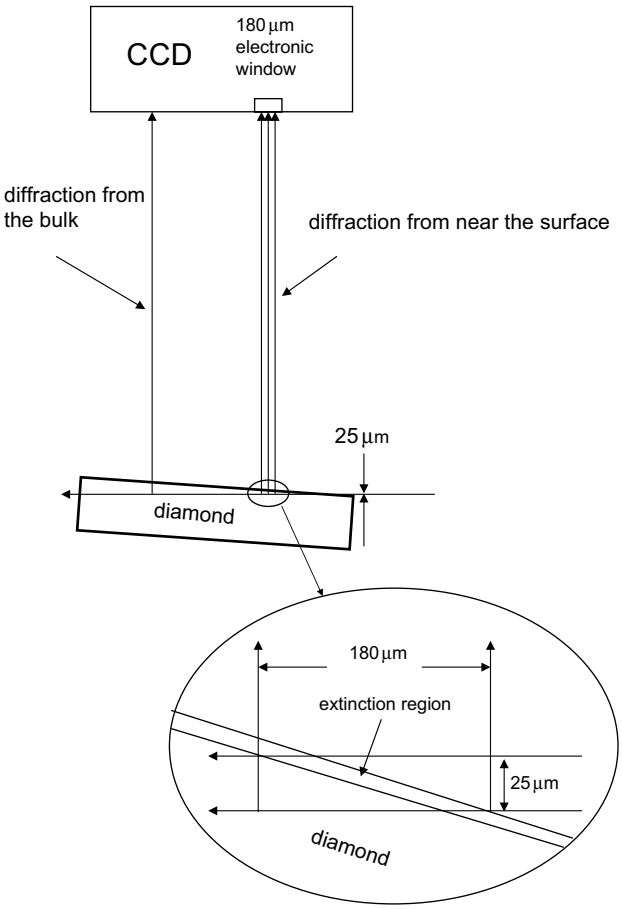

Figure 3. Microbeam topographical mode. A series of microbeam topographs was obtained by sequentially raising a diamond through a fixed beam that was sized 25 μm vertically by 6 mm horizontally. The effect was to sweep a line-shaped beam footprint from one end of the diamond to the other. Limited projection topographs were made by assembling a set of microbeam images into a patchwork image of an entire diamond. The microbeam images were assembled after applying an electronic window to the CCD data in order to reject scattering from the bulk of the crystal.

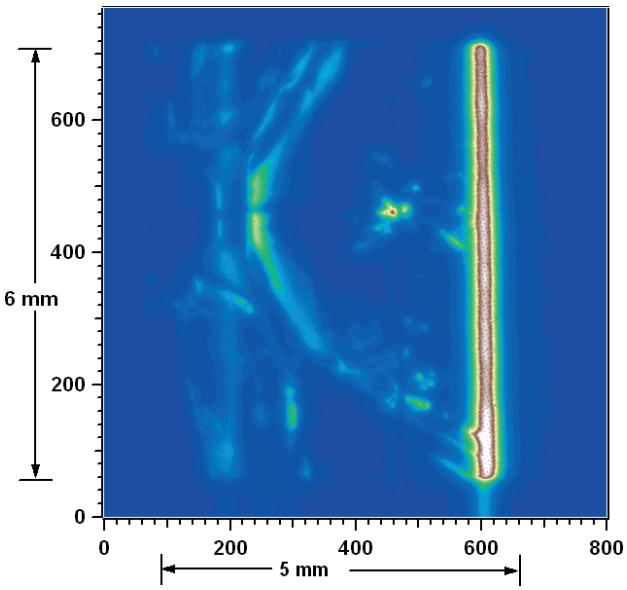

Figure 4. A topograph made in microbeam mode for a diamond with a (111) surface set to diffract from the (044) reflection at the peak of the diffraction profile. The scale values are pixel numbers. The whole diamond measured roughly 5 mm × 6 mm in size. The intensity scale is linear with increasing intensity from blue to green to yellow to brown. The strongest intensity lies in a stripe corresponding to diffraction from within 25 μm of the surface. The other features correspond to defect regions, such as growth sector boundaries. These can diffract via a part of the incident x-ray spectrum that is adjacent to that used for the stripe.

and microbeam measurements, the horizontal slit opening (∼6 mm) was sufficient to illuminate samples completely in the horizontal direction.

The microbeam mode is schematically shown in figure 3. A sample microbeam topograph is shown in figure 4. In this mode, a slit with a vertical opening of 25 μm was located upstream of the sample, and the footprint of the beam spread to either 158 or 178 μm over the surface. This resulted in an image on the CCD in which most of the intensity is concentrated into a bright stripe. The stripe corresponds to diffraction from within a depth equal to the slit opening of 25 μm, as shown in figure 3. We note that, for diamonds of high perfection, most of the intensity will arise from an extinction depth. The position of the stripe on the sample was adjusted by changing the height of the sample in the fixed beam.

The energy band pass of the Si(111) monochromator was considerably wider than that of the diamonds, so that only a portion of the incident spectrum is diffracted from a region near the surface. We note that a quite similar effect had been used in transmission to set up multiple stations in the Troika arrangement [1] at the European Synchrotron Radiation Facility. We found that we could manipulate the band pass of the Si(111) double-crystal monochromator by adjusting the angular offset of the second crystal away from parallelism with the first crystal. Also visible in figure 4 is diffraction from regions of the sample far from the stripe. This corresponds to diffraction of radiation from strained or misoriented regions that diffract x-ray energies outside a Darwin width on the energy scale.

5. Bragg-case limited projection topographs

To obtain full topographical images from the near-surface region, microbeam images in the form of stripes were assembled (i.e. 'patched') into limited projection topographs. The stripes were taken by applying a window function to the microbeam topographs. The microbeam images that formed the patchwork image were obtained sequentially as the height of the sample in the beam was stepped. The window function was set to block diffraction outside of the stripe. The window width chosen was 20 pixels, which corresponds to the footprint of the 25 μm high beam.

6. Diamond (100)/(224) results

Open beam and limited projection topographs are shown in figure 5. The sample in this case was a (100) diamond and was studied in the as-sawn state, as well as after etching.

Before etching the sample had noticeable saw grooves. These are clearly visible in the limited projection topograph

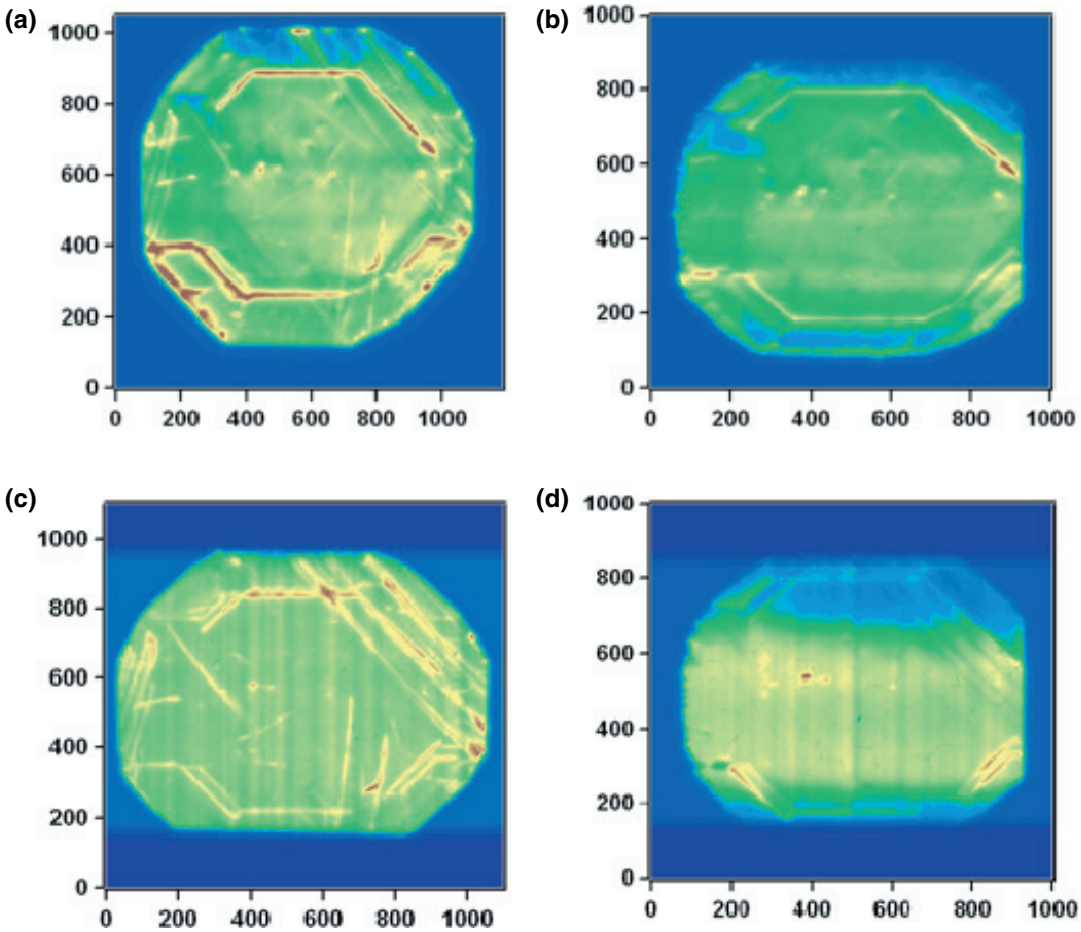

Figure 5. Topographs for a diamond with a (100) surface and procured in an as-sawed state. All topographical exposures were obtained at the peak of the diffraction profile. (*a*) A wide-beam single exposure for the as-received diamond before chemical etching. The strongest diffracted intensity was observed near growth sector boundaries that parallel the octagonal outline of the whole diamond. Diagonal saw grooves are also weakly visible. The intensity scale is linear with increasing intensity from blue to green to yellow to brown. (*b*) A wide-beam single exposure after chemical etching. (*c*) A limited projection topograph before chemical etching. The saw grooves are much more visible than in (*a*). (*d*) A limited projection topograph after chemical etching. Contrast from the saw grooves is almost completely removed.

shown in figure 5(*c*), but are less evident in the wide-beam topograph shown in figure 5(*a*). We note that the saw grooves were observable by eye and in stylus profiler measurements made on the surface. We conclude that the diamond in the region of the saw grooves was distorted so that diffraction in this region was altered. Other features visible in both types of topographs can be interpreted as intersections of growth sectors. Contrast from growth sector boundaries has been previously reported in topographical studies of diamonds [10].

A set of topographs for the same (100) diamond obtained after etching are also shown in figure 5. Both the wide-beam topograph after etching shown in figure 5(*b*), and the limited projection topograph, shown in figure 5(*d*), reveal absent or much weaker contrast from the saw grooves, and we conclude that the etch was effective in removing the saw damage.

7. Diamond (111)/(044) results

Wide-beam and limited projection topographs for a polished (111) diamond are shown in figure 6. The limited projection topograph shown in figure 6(*c*) has much stronger contrast for the growth-sector boundary than the wide-beam topograph shown in figure 6(*a*), and this contrast is significantly weakened after etching. However, triangular features were observed in the limited projection topograph obtained after etching, as shown in figure 6(*d*). These resemble the 'trigons' that other authors have reported after etching a (111) surface [11]. Corresponding triangular etch pits were also clearly visible in microscope images made with visible light.

8. Summary

We have used a 25 μm slit to obtain Bragg-case limited projection topographs of a region 25 μm below the surface. The technique was used to preferentially image surface damage. We find that a contrast corresponding to sawing grooves in a diamond plate with a (100) surface is mostly removed after chemical etching without the introduction of additional surface features. Triangular features corresponding to dislocation etch pits were observed after etching of a (111) surface.

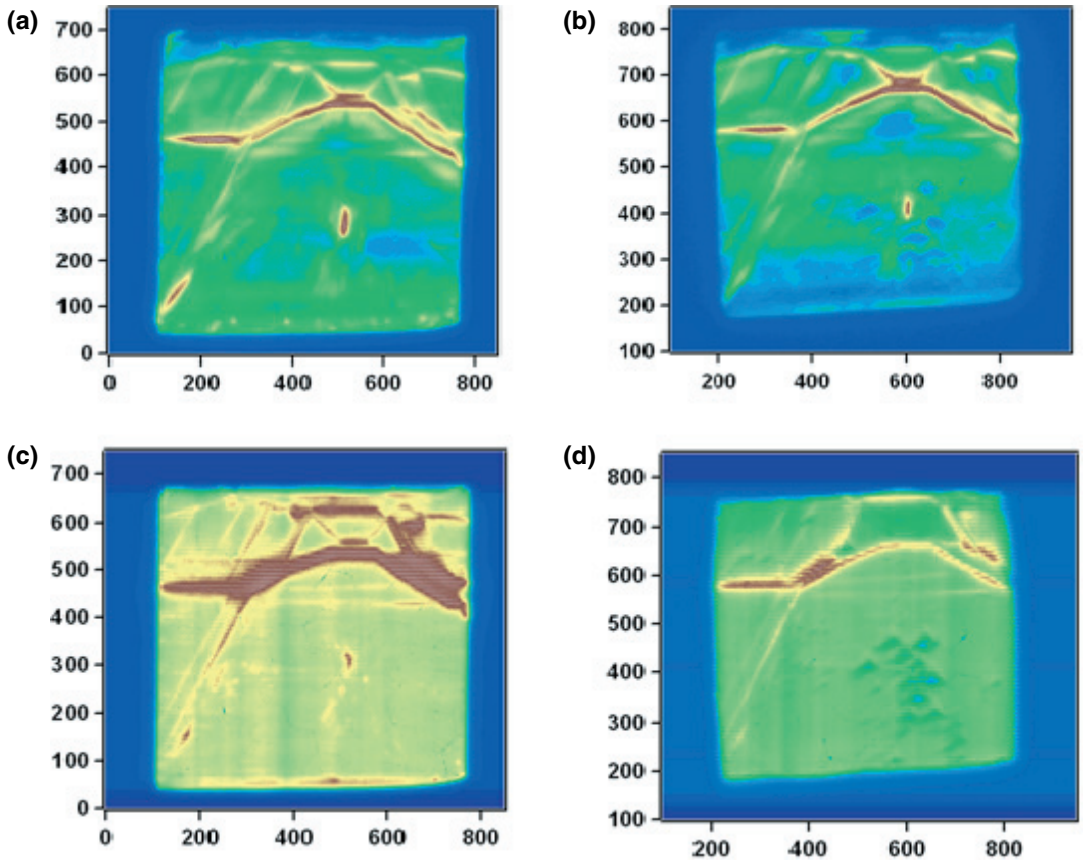

Figure 6. Topographs for (111) oriented diamond procured in a polished state. All topographical exposures were obtained at the peak of the diffraction profile. (*a*) A wide-beam single exposure for the as-received diamond before chemical etching. The intensity scale is linear with increasing intensity from blue to green to yellow to brown. The highest intensities were observed near the growth sector boundaries. (*b*) A wide-beam single-exposure topograph after chemical etching. (*c*) A limited projection topograph before chemical etching. (*d*) A limited projection topograph after chemical etching. Contrast corresponding to triangular dislocation etch pits is visible (*d*).

Acknowledgments

This work supported by the US DOE, Office of Science, Basic Energy Sciences, under Contract No W-31-109-ENG-38.

References

[1] Als-Nielsen J, Freund A K, Grubel G, Linderholm J, Nielsen M, Sanchez del Rio M and Sellschop J P F 1994 *Nucl. Instrum. Methods* B **94** 306
[2] Freund A K, Hoszowska J, Sellschop J P F, Burns R C and Rebak M 2001 *Nucl. Instrum. Methods* A **467–468** 384
[3] Maj J A, Macrander A T, Krasnicki S, Fernandez P B and Erck R A 2002 *Rev. Sci. Instrum.* **73** 1546
[4] Wierzchowski W and Moore M 1992 *Acta Phys. Pol.* A **82** 193
[5] Wieteska K *et al* 2003 *J. Phys. D: Appl. Phys* **36** A133–8
[6] Lang A R 1963 *Br. J. Appl. Phys.* **14** 904
[7] Harris/Drukker now renamed as Element 6; http://www.e6.com/
[8] Satoh S, Sumiya H, Tsuji K and Yazu S 1990 *Science and Technology of New Diamond (KTK, Tokyo)* p 351
Kiflawi I, Kanda H and Lawson S C 2002 *Diamond Relat. Mater.* **11** 204
[9] Hoszowska J, Freund A K, Boller E, Sellschop J P F, Level G, Hartwig J, Burns R C, Rebak M and Baruchel J 2001 *J. Phys. D: Appl. Phys.* **34** A47
[10] Wierzchowski W, Moore M, Makepeace A P W and Yacoot A 1991 *J. Cryst. Growth* **114** 209
[11] Patel A R and Patel S M 1968 *Br. J. Appl. Phys.* **1** 1445